COBEM 2021 26th International Congress of Mechanical Engineering
November 22-26, 2021, Virtual Congress, Brazil

COB-2021-1599
THERMODYNAMIC OPTIMIZATION OF THE ENERGY DENSITY IN AN ORGANIC RANKINE ENERGY STORAGE SYSTEM

Maury Martins de Oliveira Junior
Antônio Augusto Torres Maia
Matheus Pereira Porto
Graduate Program in Mechanical Engineering, UFMG
maurymoj@gmail.com
aamaia@demec.ufmg.br
matheuspporto@gmail.com

Abstract. The increased demand for large-scale energy storage systems to support electric grids worldwide has led to the development of new energy storage systems to mitigate the effects of the intermittent nature of both solar and wind energy. Two of the main alternatives are the Compressed Air Energy Storage (CAES) and Liquid Air Energy Storage (LAES) systems. However, CAES systems have a low energy density coupled with a high operation pressure, and LAES systems require high investment because of the air liquefaction process. The Organic Rankine Energy Storage (ORES) system has been proposed as an alternative to both of these systems as it can operate at lower pressures and closer to environment temperatures with a reasonably high round-trip efficiency (up to 73%) and relatively low cost per unit energy compared to both, CAES and LAES. However, previous models of the ORES system have only achieved an energy density of 2.3 kWh m^{-3}, lower than both that of CAES and LAES systems, 3 to 6 kWh m^{-3} and 180 kWh m^{-3}, respectively. This work aims to perform a thermodynamic optimization in an ORES system for the maximization of the round-trip efficiency and energy density. A multi-objective genetic algorithm was used in the optimization process using pressure at the high-pressure line and storage tank volumes as decision variables in a transient thermodynamic model of the ORES system. Since the performance of this system is strongly dependent on the working fluid, two fluids that have shown good results of efficiency and cost were evaluated, namely R-141b and R-365mfc. Despite the promising results in previous studies, the optimal solutions for R-365mfc obtained lower efficiencies, energy densities, and a considerably higher cost (about 25% more expensive) than those for the R-141b. A higher round-trip efficiency was obtained for R-141b, 74% compared to 63% obtained previously, however, no significant increase in energy density was achieved.

Keywords: *Thermomechanical Energy storage, Thermodynamic analysis, Organic Rankine Energy Storage, Energy density.*

1. INTRODUCTION

The demand for Energy Storage Systems (ESS) has growed considerably as a solution for the security of energy systems, particularly with scenarios of increasing shares of intermittent energy sources (mainly solar and wind) on energy grids (Aneke and Wang, 2016; Blanco and Faaij, 2018; Cebulla et al., 2018). ESS have several applications within energy grids, from long-term energy storage to frequency control, each of the applications with specific requirements (Günter and Marinopoulos, 2016; Miao Tan et al., 2021).

Pumped-hydro Energy Storage (PHES) is currently the most used solution for long-term energy storage, in terms of energy capacity, but further expansion is becoming increasingly challenging as it requires adequate geographical formations (Koohi-Fayegh and Rosen, 2020; Steinmann, 2017). That has led to the development of alternative ESS, particularly Compressed Air Energy Storage (CAES), Liquid Air Energy Storage (LAES), and Pumped Thermal Energy Storage (PTES), all with similar round-trip efficiency, (CAES between 50 and 89%, LAES between 50 and 70% and PTES between 53 to 80%) all lower than PHES (Aneke and Wang, 2016; Argyrou et al., 2018; Benato and Stoppato, 2018a; Koohi-Fayegh and Rosen, 2020). CAES has a more mature technology but also requires a suitable geographical formation while LAES involves a liquefaction process that results in a higher system cost and limited efficiency (Koohi-Fayegh and Rosen, 2020; Olympios et al., 2021). PTES is a more recent ESS but has shown promising results and already has a pilot plant, but preliminary results indicate it might have a higher cost per unit energy and per unit power (Georgiou et al., 2018).

Recently, the Organic Ranking Energy Storage (ORES) system has also been proposed and evaluated considering commonly used organic fluids as the working fluids with a competitive round-trip efficiency in an initial study (Oliveira Jr et al., 2020). The main objective of this work is to use multi-objective optimization methods to maximize energy density and round-trip efficiency of an ORES systems while maintaining a competitive round-trip efficiency through the variation

of storage volume and pressure at the turbine inlet. The optimization was applied to the ORES system for two different fluids and the influence of the variations on the operational parameters on the system CAPEX (Capital Expenditure) was also be evaluated.

2. THERMODYNAMIC ANALYSIS

The ORES system consists of two stages, an energy charging phase and an energy discharging phase. The ORES discharging phase is shown in Figure 1, with active lines in black and inactive lines in grey.

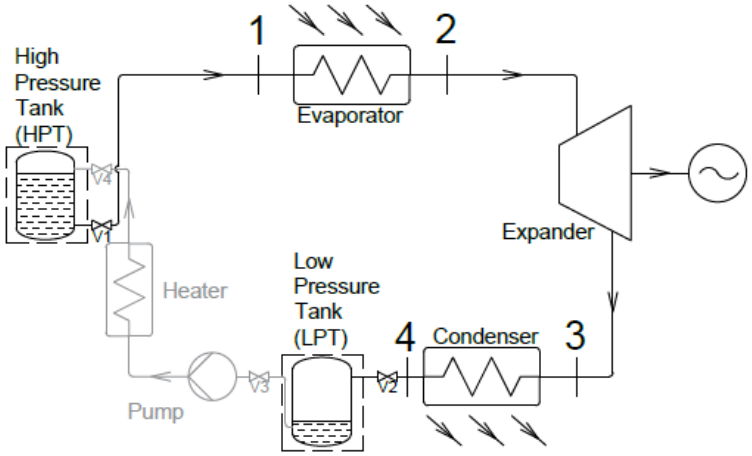

Figure 1 – ORES discharging phase schematics (active lines in black).

During the discharging phase, the fluid is released from the high-pressure storage tank (HPT) and receives heat in an evaporator before entering in the expander. The specific heat received at the evaporator q_{Ev} can be obtained from an energy balance on the control volume of the evaporator, resulting in Eq. (1),

$$\mathrm{q_{Ev}} = h_2 - h_1, \tag{1}$$

where h_2 and h_1 are the enthalpies at the outlet and inlet of the evaporator, respectively. The specific enthalpy at the outlet of the expander can be estimated from Eq. (2),

$$\mathrm{h_3} = h_2 + \eta_{Ex}(h_2 - h_{3,s}), \tag{2}$$

where η_{Ex} is the isoentropic efficiency of the expander and $h_{3,s}$ is the enthalpy at the expander outlet for an isoentropic expansion. Finally, the specific work produced in the expander can be estimated with an energy balance applied to the control volume of the expander, resulting in Eq. (3)

$$w_{Ex} = h_3 - h_2. \tag{3}$$

Then the working fluid goes through a condenser before reaching the low-pressure storage tank (LPT). The specific heat removed in the condenser is then obtained with another energy balance, now applied to a control volume around the condenser, Eq. (4)

$$q_c = h_3 - h_4. \tag{4}$$

The mass flow rate during the discharging phase, $\dot{m}_D$, can be obtained as a function of the expander power $\dot{W}_{Ex}$, Eq. (5),

$$\dot{m}_D = \frac{\dot{W}_{Ex}}{w_{Ex}}. \tag{5}$$

As the HPT storage tank is discharged, the thermodynamic states in both the LPT and HPT change, which leads to a change in both the high and low-pressure lines. Applying energy and mass balances at the HPT and LPT control volumes results in Eqs. (6) to (9),

$$\frac{D(m_{HPT})}{dt} = -\dot{m}_D, \tag{6}$$

$$\frac{D(U_{HPT})}{dt} = -\dot{m}_D\, h_{l,HPT}, \tag{7}$$

$$\frac{D(m_{LPT})}{dt} = \dot{m}_D, \tag{8}$$

$$\frac{D(U_{LPT})}{dt} = \dot{m}_D\, h_4, \tag{9}$$

where U_{HPT} and U_{LPT} are the total internal energy in the HPT and LPT, respectively, m_{HPT} and m_{LPT} are the total mass of fluid in the HPT and LPT, respectively, and $h_{l,HPT}$ is the specific energy of the saturated liquid at the HPT.

The ORES discharging phase is shown in Figure 2, with active lines in black and inactive lines in grey.

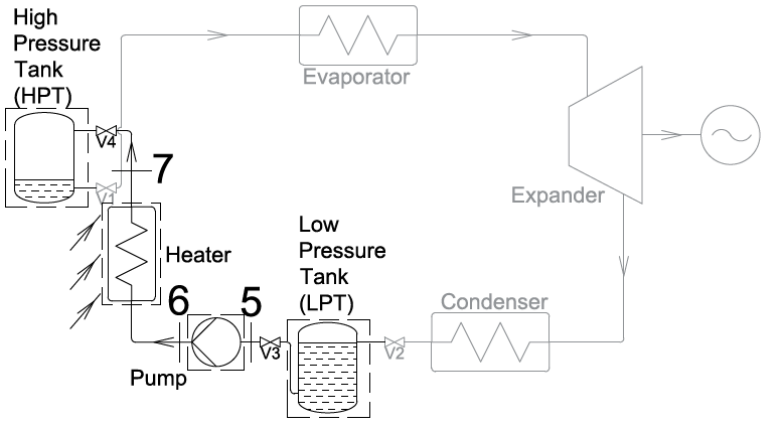

Figure 2 – ORES charging phase schematics (active lines in black).

The state at the pump outlet can be found with an energy balance on the pump, Eq. (10),

$$\mathrm{h}_6 = h_5 + \frac{h_{6,s} - h_5}{\eta_p}, \tag{10}$$

where η_P is the isoentropic efficiency of the pump and $h_{6,s}$ is the enthalpy at the pump outlet in an isoentropic compression. Finally, the specific work provided by the pump w_P is given by Eq. (11),

$$w_P = h_6 - h_5. \tag{11}$$

The mass flow rate at the charging phase, $\dot{m}_{Ch}$, can be then obtained as a function of the power provided by the pump $\dot{W}_P$, Eq. (12),

$$\dot{m}_{Ch} = \frac{\dot{W}_P}{w_P}. \tag{12}$$

The working fluid is then heated before returning to the HPT. The specific heat added to the heater q_H can then be obtained using an energy balance on the control volume of the heater, Eq. (13)

$$q_H = h_7 - h_6. \tag{13}$$

Just as with the discharging phase, the thermodynamic states at the tanks also change during the charging phase, and a balance of mass and energy on the storage tanks leads to a similar set of equations, Eqs. (14) to (17),

$$\frac{d(m_{HPT})}{dt} = \dot{m}_{Ch}, \tag{14}$$

$$\frac{d(U_{HPT})}{dt} = \dot{m}_{Ch}\, h_7, \tag{15}$$

$$\frac{d(m_{LPT})}{dt} = -\dot{m}_{Ch}, \tag{16}$$

$$\frac{d(U_{LPT})}{dt} = -\dot{m}_{Ch}\, h_{l,LPT}, \tag{17}$$

where $h_{l,LPT}$ is the specific enthalpy of the saturated liquid leaving the LPT.

The heat required in the evaporator and heater were provided by two heat pumps, HP1 and HP2, respectively. The energy required by each of the heat pumps, both obtained from the definition of the coefficient of performance, Eqs. (18) and (19),

$$W_{HP1} = \frac{Q_{Ev}}{COP_{HP1}}, \tag{18}$$

$$W_{HP2} = \frac{Q_H}{COP_{HP2}}, \tag{19}$$

where COP_{HP1} and COP_{HP2} are the coefficients of performance for HP1 and HP2, respectively.

Finally, the round-trip efficiency η_{RT} of the system is defined as the ratio between the net energy generated during the discharging phase and the energy consumed in the charging phase, Eq. (20),

$$\eta_{RT} = \frac{W_{Ex} - W_{HP1}}{W_P + W_{HP2}}, \tag{20}$$

and the energy density (in terms of volume) as the ratio of produced energy by storage volume, and is given by Eq. (21)

$$\rho_{E_V} = \frac{W_{Ex}}{V_{HPT} + V_{LPT}}, \tag{21}$$

where V_{LPT} and V_{HPT} are the low pressure and high pressure storage tanks, respectively.

3. COST ANALYSIS

The CAPEX (Capital Expenditure) of the system will be estimated considering its main components, namely expander, pressure vessels, pump, working fluid, and auxiliary equipment. Therefore, the CAPEX can be estimated with Eq. (22),

$$CAPEX = C_{fl} + C_{St} + C_{Ex} + C_p + C_{aux}, \tag{22}$$

where C_{fl} is the cost of the working fluid, C_{st} is the cost of the storage vessels, C_{Ex} is the cost of the expander, C_p the cost of the pump and C_{aux} is the cost of the auxiliary components. The cost of the pump, expander, and storage vessels are estimated using the Bare Module Cost method (Turton et al., 2018). C_{Ex} can be estimated as a function of the power $\dot{W}_{Ex}$, type of expander and expander material, Eqs. (23) and (24),

$$C_{Ex} = C_{0,Ex} F_{M,Ex}, \tag{23}$$

$$\log C_{0,Ex} = K_{1,Ex} + K_{2,Ex} \log \dot{W}_{Ex} + K_{3,Ex} \left(\log \dot{W}_{Ex}\right)^2, \tag{24}$$

where $F_{M,Ex}$ is the material factor of the expander, and $K_{1,Ex}$, $K_{2,Ex}$ and $K_{3,Ex}$ are coefficients associated with the type of expander. The cost of the pump can be estimated as a function of the power $\dot{W}_p$, pressure P_P and pump material, Eqs. (25) to (27),

$$C_p = C_{0,p}\left[B_{1,p} + \left(B_{2,p}\, F_{M,p}\, F_{P,p}\right)\right], \tag{25}$$

$$\log C_{0,p} = K_{1,p} + K_{2,p} \log \dot{W}_p + K_{3,p}\left(\log \dot{W}_p\right)^2, \tag{26}$$

$$\log F_{P,p} = C_{1,p} + C_{2,p} \log P_p + C_{3,p}\left(\log P_p\right)^2, \tag{27}$$

where $F_{M,p}$ is the material factor for the pump, and $K_{1,p}$, $K_{2,p}$, $K_{3,p}$, $C_{1,p}$, $C_{2,p}$ and $C_{3,p}$ are coefficients for the pump. The cost for each storage vessel can be obtained with Eqs. (28) to (30),

$$C_{St} = C_{0,St}\left[B_{1,St} + \left(B_{2,St}\, F_{M,St}\, F_{P,St}\right)\right], \tag{28}$$

$$\log C_{0,St} = K_{1,St} + K_{2,St} \log V + K_{3,St} (\log V)^2, \tag{29}$$

$$\log F_{P,St} = \frac{\dfrac{P_{barg} D_i}{2\, S\, E - 1.2\, P_{barg}} + CA}{t_{min}}, \tag{30}$$

where V is the storage volume in m^3, $F_{M,St}$ is the material factor for the storage vessel, P_{barg} is the pressure gauge in bar, D_i is the internal diameter of the storage vessel, S is the maximum allowable tension, E is the welded joint efficiency, CA is the corrosion allowance and t_{min} is the minimum tank thickness. The coefficients for Eqs. (23) to (30) are shown in Table 1, considering the use of a stainless steel axial turbine, carbon steel centrifugal pump and a vertical carbon steel storage tank.

Table 1 – Coefficients of the bare module cost equations for a centrifugal pump, axial turbine and storage tank cost (Kazemi and Samadi, 2016; Le et al., 2014; Pezzuolo et al., 2016; Turton et al., 2018).

	B_1	B_2	K_1	K_2	K_3	C_1	C_2	C_3	F_M
Expander	-	-	2.7051	1.4398	-0.1776	-	-	-	6.2
Pump	1.89	1.35	3.3892	0.0536	0.1538	-0.3935	0.3957	-0.00226	1.6
Storage tank	2.25	1.82	3.4974	0.4485	0.1074	-	-	-	1.0

The equations for the estimation of the costs, Eqs. (22) to (30), are developed based on historic price data for each of the components and must be updated based on inflation indexes I, the most common of which for this type of application is the CEPCI. Cost values are updated from year i to year j using Eq. (31),

$$C_j = C_i \left(\frac{I_j}{I_i}\right). \tag{31}$$

4. METHODOLOGY

The R-141b and R-365mfc were selected for this study given their promising results in previous studies (Oliveira Jr et al., 2020), their main properties are summarized in Table 2.

Table 2 – Properties of the evaluated working fluids (Bell et al., 2014; Oliveira Jr et al., 2020).

Fluid	Molar mass [kg/kmol]	T_{crit} [K]	P_{crit} [kPa]	ODP	GWP (100 yrs)	Cost [USD/kg]
R-365mfc	148.08	460.00	3,266	0	794	6.68
R-141b	116.95	477.50	4,249	0.120	725	4.22

The optimization process was implemented for the maximization of the energy density and round-trip efficiency using a multi-objective genetic algorithm. The pressure at the high-pressure line and the volumes of the storage tanks were selected as the decision variables. The thermodynamic model presented in the previous section was used to develop a transient analysis model using the Euler explicit method to simplify the differential equations, Eqs. (6) to (9) and Eqs. (14) to (17), for the calculations of the energy density and efficiency resulting in Eqs. (32) to (35) for the discharging process and Eqs. (36) to (39) for the charging process,

$$m_{HPT}^{t_i} = m_{HPT}^{t_{i-1}} - \dot{m}_D\, dt, \tag{32}$$

$$U_{HPT}^{t_i} = U_{HPT}^{t_{i-1}} - \dot{m}_D \, h_{l,HPT}^{t_{i-1}} \, dt, \tag{33}$$

$$m_{LPT}^{t_i} = m_{LPT}^{t_{i-1}} + \dot{m}_D \, dt, \tag{34}$$

$$U_{LPT}^{t_i} = U_{LPT}^{t_{i-1}} + \dot{m}_D \, h_4^{t_{i-1}} \, dt, \tag{35}$$

$$m_{HPT}^{t_i} = m_{HPT}^{t_{i-1}} + \dot{m}_{Ch} \, dt, \tag{36}$$

$$U_{HPT}^{t_i} = U_{HPT}^{t_{i-1}} + \dot{m}_{Ch} \, h_7^{t_{i-1}} \, dt, \tag{37}$$

$$m_{LPT}^{t_i} = m_{LPT}^{t_{i-1}} - \dot{m}_{Ch} \, dt, \tag{38}$$

$$U_{LPT}^{t_i} = U_{LPT}^{t_{i-1}} - \dot{m}_{Ch} \, h_{l,LPT}^{t_{i-1}} \, dt, \tag{39}$$

where t_i is the time at instant i, t_{i-1} is the time at the previous instant and dt is the time step. Figure 3 shows the fluxogram for the transient model algorithm of the system using K_{HPT}, K_{LPT} and P_H as the input variables.

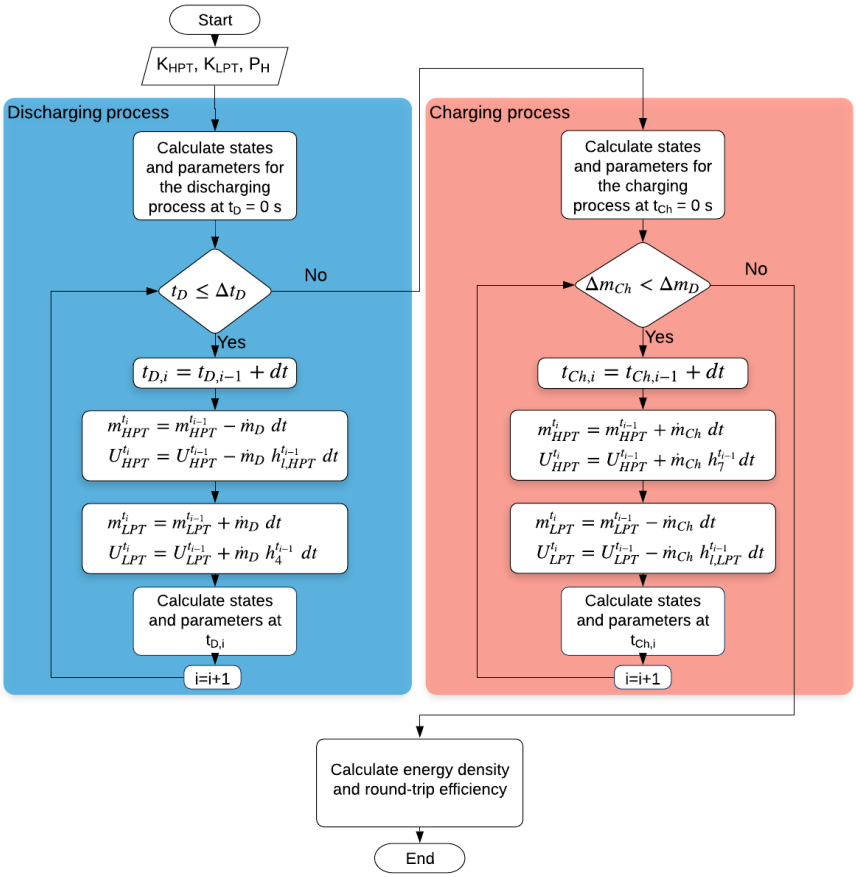

Figure 3 – Flowchart for the transient model algorithm.

A quasi-steady-state model, assuming dE/dt = 0 and dm/dt = 0 (essentially the same as considering tanks with infinite volumes), was also used for the calculation of the round-trip efficiency as a constraint for the optimization, this was done to reduce the computational cost of the optimization process.

The volume required at the tanks is dependent on the fluid and its thermodynamic state at the storage tank, therefore, a Minimum Design Volume (MDV) was defined for both the LPT and HPT. The MDV for the HPT for a system with a discharge process with duration Δt_D was defined as the volume required such that the quality at the HPT would vary from 0.02 up to 0.98 and considering that the mass flow rate at $t = 0$, $\dot{m}_D^{t=0}$ would remain constant over the entire discharging

process. The MDV for the LPT is similar but with a quality of 0.98 at the start and 0.02 at the end of the discharging process, as defined by Eqs. (40) and (41), respectively,

$$MDV_{HPT} = \frac{\dot{m}_D^{t=0}\,\Delta t_D}{\rho_{HPT}^{t=0} - \rho_{HPT}^{t=t_{end}}}, \tag{40}$$

$$MDV_{LPT} = \frac{\dot{m}_D^{t=0}\,\Delta t_D}{\rho_{LPT}^{t=0} - \rho_{LPT}^{t=t_{end}}}. \tag{41}$$

where $\rho_{HPT}^{t=0}$ and $\rho_{HPT}^{t=t_{end}}$ are the specific mass of the HPT at the start and end of the discharging phase, respectively, and $\rho_{LPT}^{t=0}$ and $\rho_{LPT}^{t=t_{end}}$ the same for the LPT. The volumes of the HPT and LPT can then be set based on multiplication factors, K_{V_H} and K_{V_L}, respectively, i.e. $V_{HPT} = K_{V_H}\,MDV_{HPT}$ and $V_{LPT} = K_{V_L}\,MDV_{LPT}$.

The volume coefficients for both the low-pressure tank, K_{V_L}, and high-pressure tank, K_{V_H}, were constrained between 1.2 and 4.0 while the pressure on the high-pressure line was constrained to values between 5% higher than the ambient saturation pressure and 95% of the critical pressure of the working fluid, as the study was limited to sub-critical conditions for both fluids. Another constraint was that the round-trip efficiency of the steady-state analysis needs to be higher than 50%, so that the system remains competitive with other long-term energy storage systems (Argyrou et al., 2018; Benato and Stoppato, 2018b; Koohi-Fayegh and Rosen, 2020). This optimization provides a Pareto front (a set of optimal solutions) that will then be used to calculate the CAPEX associated with each of these solutions with Eqs. (22) to (31) and updating the cost to 2019 (Scott Jenkins, 2019). The models of the system were implemented in MATLAB with the CoolProp external library for the thermodynamic properties(Bell et al., 2014). The assumptions and system parameters considered for these analyses are summarized in Table 3.

Table 3 - Assumptions and pre-defined parameters (Hærvig et al., 2016; Lecompte et al., 2015).

Ambient temperature, T_{amb}	25 ºC
Ambient pressure, P_{amb}	101.3 kPa
Discharge phase duration, Δt_D	1 h
Expander power, $\dot{W}_{Ex}$	1,000 kW
Pump power, $\dot{W}_p$	200 kW
Expander isoentropic efficiency, η_{Ex}	0.80
Pump isoentropic efficiency, η_p	0.75
Isobaric heating and cooling	
Negligible pressure loss	

5. RESULTS AND ANALYSIS

The Pareto fronts for the optimizations of the ORES system using R-365mfc and R-141b are shown in Figure 4.

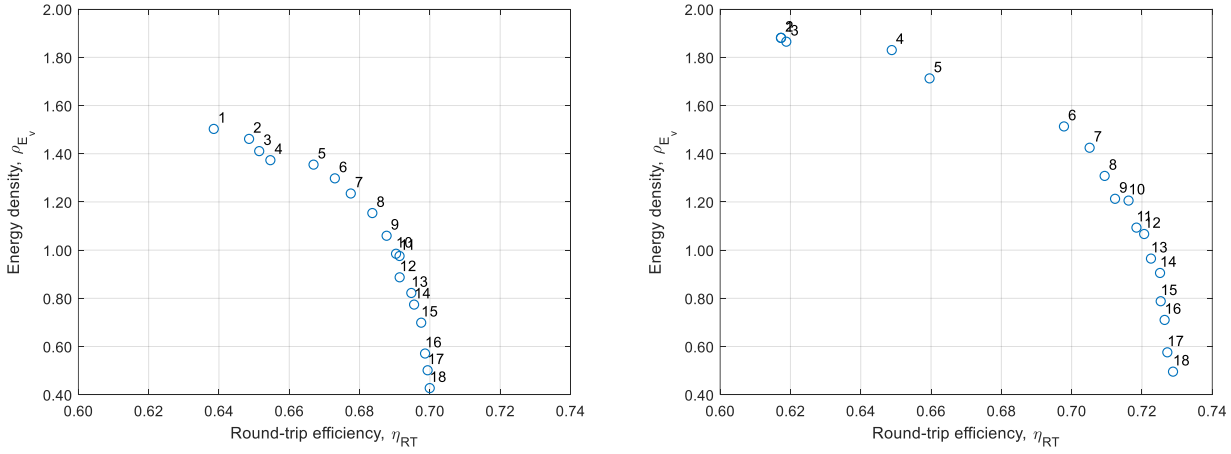

(a) R-365mfc (b) R-141b

Figure 4 – Pareto fronts (Set of optimal solutions).

R-141b has surpassed R-365mfc both in terms of efficiency (the maximum efficiency for R-365mfc was around 70% while R-141b reached an efficiency of around 73%) and in terms of density (maximum density for R-365mfc was 1.5

kWh m^{-3} and 1.9 kWh m^{-3} for R-141b). More than that, for every optimal solution for the R-365mfc, there is at least one solution for the R-141b that has higher efficiency for a similar energy density or higher density for a similar efficiency, therefore the solutions for R-141b have fully dominated the solutions for R-365mfc. Then the costs of the systems for each of the optimal solutions were calculated, again for both fluids. Figure 5 shows the cost for each optimal solution obtained with the multiobjective genetic algorithm for R-365mfc, ordered from smallest to highest η_{RT}, with the proportions of the cost with each of its components followed by the values of their objective functions (efficiency and energy density) and their respective set of decision variables (K_{V_H}, K_{V_L} and P_H).

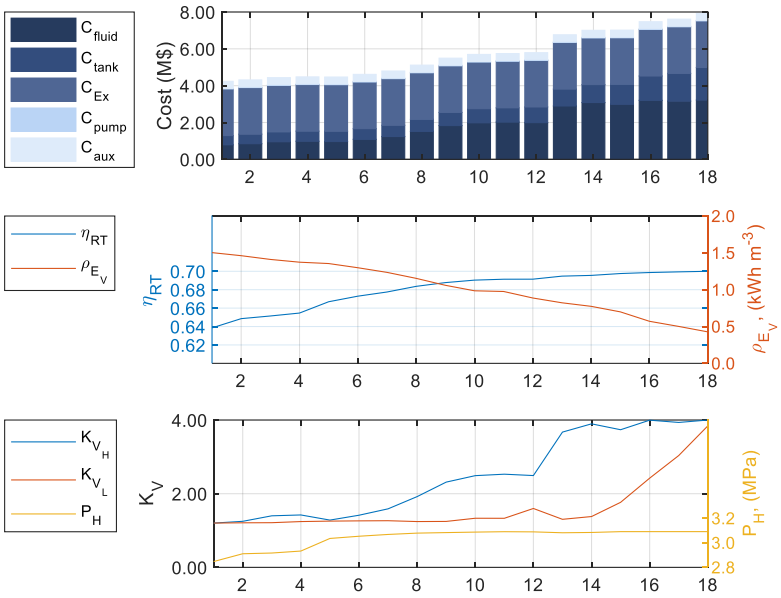

Figure 5 – CAPEX divided by component, values of the objective functions (η_{RT} and ρ_{E_V}) and decision variables (K_{V_H}, K_{V_L} and P_H) for R-365mfc.

The cost of the system increases significantly as systems achieved higher efficiencies, even doubling the value for the system with lower efficiency, mainly due to the increased cost of the storage tank (greater volume and pressure at the tank) and the cost of the fluid, both achieving almost triple their cost than in the lower efficiency system. While the cost of the systems with higher energy density was composed mainly by the expander with a small contribution of the tanks and fluid. The main component of cost for the higher efficiency system was the cost of the fluid, followed by expander and then storage tank. Figure 6 shows the cost for each optimal solution for R-141b followed by the values of their objective functions (efficiency and energy density) and the set of decision variables (K_{V_H}, K_{V_L} and P_H).

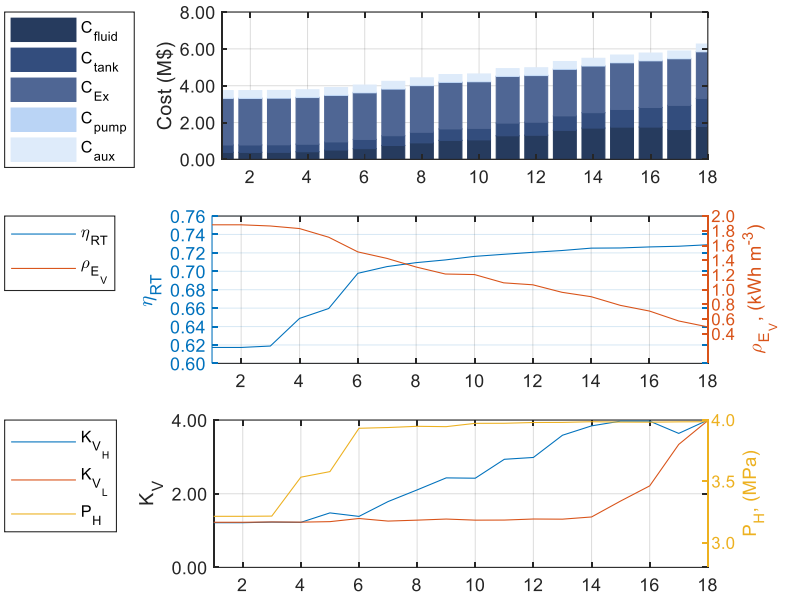

Figure 6 – CAPEX divided by component, values of the objective functions (η_{RT} and ρ_{EV}) and decision variables (K_{V_H}, K_{V_L} and P_H) for R-141b.

Although the pattern remained similar, the increase in cost with the increased efficiency was smaller than for R-365mfc, with the expander remaining the main component of cost for all systems, despite the operation at higher pressures.Both fluids also had a similar composition of the decision variables, with low storage volumes and relatively lower pressures for the systems with higher energy density and a higher volume storage and pressures closer to the critical pressure for high efficiency systems. The volume in the low pressure tank, however, was kept around its minimum value for most of the optimal solutions except for the three highest efficiency systems for both fluids, indicating its smaller influence on system efficiency. Both fluids had an almost linear decrease in energy density while increases in efficiency became slower, indicating an operational limit for η_{RT} at around 71% for R-365mfc and 74% for R-141b. The gradient for the energy efficiency became apparently lower closer to the intersection point of the energy density and round-trip efficiency curves, indicating a promising operational point as it represented a compromise between energy density and efficiency,with a decrease of around 26% in density for both fluids and an increase of 8% and 14% in efficiency for R-365mfc and R-141b, respectively, and around 6% increase in CAPEX for both fluids.

6. CONCLUSIONS

This study has implemented a multi-objective optimization for the maximization of the round-trip efficiency and energy density of an ORES system comparing the operation using R-365mfc and R-141b as a working fluid and using the volumes of the storage tanks and the pressure at the high-pressure line as decision variables. Despite the better performance of R-365mfc in previous studies, R-141b has surpassed it in terms of efficiency, energy density and even CAPEX, demonstrating a better working fluid option for the ORES systems under the conditions investigated in this study. As expected, both fluids obtained higher efficiencies for systems with higher storage volumes and operating at higher pressures, resulting in lower energy densities, R-365mfc reached an efficiency of 71% that corresponded to an energy density of 0.4 kWh m^{-3} and R-141b reached 74% with an energy density of 0.5 kWh m^{-3}. While the higher densities were obtained for lower volumes and pressures, 1.5 kWh m^{-3} and 64 % for R-365mfc and 1.9 kWh m^{-3} and 62 % for R-141b. The intersection points of the curves of energy density and round-trip efficiency were considered potential operational points as they represented a compromise in energy density and efficiency for both fluids with an increase of 6% in CAPEX. The intersection point was reached after a decrease of approximately 26 % for both fluids that represented an increase in round-trip efficiency of 8% for R-365mfc and 14% for R-141b.

7. ACKNOWLEDGEMENTS

This study was financed in part by the Coordenação de Aperfeiçoamento de Pessoal de Nível Superior – Brasil (CAPES) - Finance Code 001, and by the CNPq (Conselho Nacional de Desenvolvimento Científico e Tecnológico - Brazil).

8. REFERENCES

Aneke, M., Wang, M., 2016. Energy storage technologies and real life applications – A state of the art review. Appl. Energy 179, 350–377. https://doi.org/10.1016/j.apenergy.2016.06.097

Argyrou, M.C., Christodoulides, P., Kalogirou, S.A., 2018. Energy storage for electricity generation and related processes: Technologies appraisal and grid scale applications. Renew. Sustain. Energy Rev. 94, 804–821. https://doi.org/10.1016/J.RSER.2018.06.044

Bell, I.H., Wronski, J., Quoilin, S., Lemort, V., 2014. Pure and pseudo-pure fluid thermophysical property evaluation and the open-source thermophysical property library coolprop. Ind. Eng. Chem. Res. 53, 2498–2508. https://doi.org/10.1021/ie4033999

Benato, A., Stoppato, A., 2018a. Pumped Thermal Electricity Storage: A technology overview. Therm. Sci. Eng. Prog. https://doi.org/10.1016/j.tsep.2018.01.017

Benato, A., Stoppato, A., 2018b. Heat transfer fluid and material selection for an innovative Pumped Thermal Electricity Storage system. Energy 147, 155–168. https://doi.org/10.1016/J.ENERGY.2018.01.045

Blanco, H., Faaij, A., 2018. A review at the role of storage in energy systems with a focus on Power to Gas and long-term storage. Renew. Sustain. Energy Rev. 81, 1049–1086. https://doi.org/10.1016/J.RSER.2017.07.062

Cebulla, F., Haas, J., Eichman, J., Nowak, W., Mancarella, P., 2018. How much electrical energy storage do we need? A synthesis for the U.S., Europe, and Germany. J. Clean. Prod. 181, 449–459. https://doi.org/10.1016/J.JCLEPRO.2018.01.144

Georgiou, S., Shah, N., Markides, C.N., 2018. A thermo-economic analysis and comparison of pumped-thermal and liquid-air electricity storage systems. Appl. Energy 226, 1119–1133. https://doi.org/10.1016/j.apenergy.2018.04.128

Günter, N., Marinopoulos, A., 2016. Energy storage for grid services and applications: Classification, market review, metrics, and methodology for evaluation of deployment cases. J. Energy Storage 8, 226–234. https://doi.org/10.1016/J.EST.2016.08.011

Hærvig, J., Sørensen, K., Condra, T.J., 2016. Guidelines for optimal selection of working fluid for an organic Rankine cycle in relation to waste heat recovery. Energy 96, 592–602. https://doi.org/10.1016/j.energy.2015.12.098

Kazemi, N., Samadi, F., 2016. Thermodynamic, economic and thermo-economic optimization of a new proposed organic Rankine cycle for energy production from geothermal resources. Energy Convers. Manag. 121, 391–401. https://doi.org/10.1016/j.enconman.2016.05.046

Koohi-Fayegh, S., Rosen, M.A., 2020. A review of energy storage types, applications and recent developments. J. Energy Storage. https://doi.org/10.1016/j.est.2019.101047

Le, V.L., Kheiri, A., Feidt, M., Pelloux-Prayer, S., 2014. Thermodynamic and economic optimizations of a waste heat to power plant driven by a subcritical ORC (Organic Rankine Cycle) using pure or zeotropic working fluid. Energy 78, 622–638. https://doi.org/10.1016/j.energy.2014.10.051

Lecompte, S., Huisseune, H., van den Broek, M., Vanslambrouck, B., De Paepe, M., 2015. Review of organic Rankine cycle (ORC) architectures for waste heat recovery. Renew. Sustain. Energy Rev. 47, 448–461. https://doi.org/10.1016/j.rser.2015.03.089

Miao Tan, K., Sudhakar Babu, T., Ramachandaramurthy, V.K., Kasinathan, P., Solanki, S.G., Raveendran, S.K., 2021. Empowering smart grid: A comprehensive review of energy storage technology and application with renewable energy integration. J. Energy Storage 39, 102591. https://doi.org/10.1016/j.est.2021.102591

Oliveira Jr, M.M., Maia, A.A.T., Porto, M.P., 2020. Organic Rankine Energy Storage (ORES) system. Energy 204. https://doi.org/10.1016/j.energy.2020.117938

Olympios, A. V, McTigue, J.D., Farres-Antunez, P., Tafone, A., Romagnoli, A., Li, Y., Ding, Y., Steinmann, W.-D., Wang, L., Chen, H., Markides, C.N., 2021. Progress and prospects of thermo-mechanical energy storage—a critical review. Prog. Energy 3, 022001. https://doi.org/10.1088/2516-1083/abdbba

Pezzuolo, A., Benato, A., Stoppato, A., Mirandola, A., 2016. The ORC-PD: A versatile tool for fluid selection and Organic Rankine Cycle unit design. Energy 102, 605–620. https://doi.org/10.1016/j.energy.2016.02.128

Scott Jenkins, 2019. CHEMICAL ENGINEERING PLANT COST INDEX: 2018 ANNUAL VALUE [WWW Document]. Chem. Eng. URL https://www.chemengonline.com/2019-cepci-updates-january-prelim-and-december-2018-final/ (accessed 6.12.21).

Steinmann, W.-D., 2017. Thermo-mechanical concepts for bulk energy storage. Renew. Sustain. Energy Rev. 75, 205–219. https://doi.org/10.1016/j.rser.2016.10.065

Turton, R., Shaeiwitz, J.A., Bhattacharyya, D., Whiting, W.B., 2018. Analysis, synthesis, and design of chemical processes, 5th editio. ed. Pearson Education, Inc.

9. RESPONSIBILITY NOTICE

The authors are the only responsible for the printed material included in this paper.